PCCP

Accepted Manuscript

ROYAL SOCIETY OF CHEMISTRY

www.rsc.org/pccp

Water Inhibits CO Oxidation on Gold Cations in the Gas Phase. Structures and Binding Energies of the Sequential Addition of CO, H_2O, O_2, and N_2 onto Au^+

J. Ulises Reveles[1], Khaled M. Saoud[2] and M. Samy El-Shall[*3]

[1]Physics Department and [3]Chemistry Department, Virginia Commonwealth University, Richmond, Virginia 23284-2000

[2]Liberal Arts and Sciences Program, Virginia Commonwealth University in Qatar, Doha, Qatar

Graphical Abstract

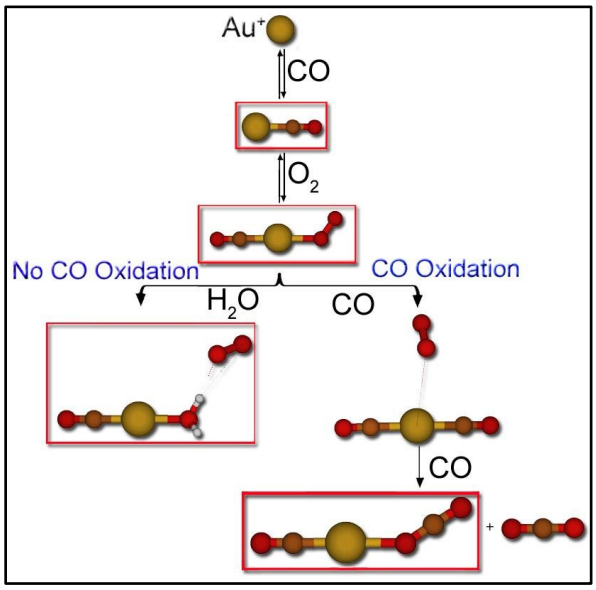

ABSTRACT

We report a detailed experimental and theoretical study of the gas phase reactivity of Au^+ with CO, O_2, N_2 and their mixtures in the presence of a trace amount of water impurity. The gold cation is found to strongly interact with CO and H_2O molecules via successive addition reactions until reaching saturation. The stoichiometry of the formed complex is determined by the strength of the binding energy of the neutral molecule to the gold cation. CO binds the strongest to Au^+, followed by H_2O, N_2 and then O_2. We found that the gold cation (Au^+) can activate the O_2 molecule within the $Au^+(CO)_2(O_2)$ complex which could react with another CO molecule to form $Au^+(CO)(CO_2)$ + CO_2. The product $Au^+(CO)(CO_2)$ is observed experimentally with a small intensity at room temperature. However, the presence of water leads to the formation of $Au^+(CO)(H_2O)(O_2)$ instead of $Au^+(CO)_2(O_2)$ due to the strong interaction between Au^+ and water. The current experiments and calculations might lead to a molecular level understanding of the interactions between the active sites, reactants and impurities which could pave the way for the design of efficient nanocatalysts.

---

*Corresponding Author: mselshal@vcu.edu, Tel: +8048282753

1. INTRODUCTION

The pressure gap between surface science and heterogeneous catalysis is a very important issue in catalysis. It is found that surface science experiments on well-defined surfaces in ultra-high vacuum (UHV) conditions yield results that are different from results obtained in high-pressure catalytic reactors. For example, for the catalytic CO oxidation on ruthenium at a total pressure > 10 torr, for which the rate of CO oxidation on Ru(001) is higher than on any other transition metal surface, it is found that the oxidation rate is highest for a combination of high surface coverage of oxygen and extremely low coverage of CO.[1,2] In contrast, Ru(001) is among the poorest catalysts for CO oxidation under UHV conditions.[3]

In heterogeneous catalysis typical supported catalysts consisting of metal nanoparticles dispersed on high-surface area support materials are quite complex and difficult to characterize in detail. For example, in typical CO oxidation catalysts, such as gold nanoparticles supported on metal oxides, it is difficult to obtain mechanistic insights into the role of the metal nanoparticle size, degree of oxidation and the nature of metal-support interaction.[1,2] Size-selected cluster deposition experiments showed significant activity and size dependence of small gold clusters as small as seven or eight atoms.[4-6]

Gas phase reactions of metal ions with different molecules under typical reaction conditions can provide useful information about the intrinsic properties of metal ions and their reactivity.[7-15] Valuable information such as reaction mechanisms, reaction rates, and thermochemistry can be obtained using these types of experiments coupled with high level theoretical calculations. This can result in a molecular level understanding the crucial reaction steps and complete characterization of the reaction intermediates which ultimately can improve the design of efficient catalyst systems.[16] The advantages of gas phase reactions in catalysis arise from the possibility of elucidating basic properties of isolated molecules and probing reactions under well-defined conditions since they are not hampered by different disturbing factors in solution such as association by ion pairing, solvent–shell interactions, intra and inter-molecular processes that lead to distraction, and/or modification of the catalytically active species.[17]

Research on the catalytic activity of gold nanoparticles was fueled by the seminal work of Haruta *et al.* which reported on the unexpected low-temperature catalytic activity of gold clusters towards CO oxidation.[18,19] In addition to particle size and support effects, oxidation state has been noted as one of the main factors that affect the catalytic activity,[20-22] and ionic gold has

been known to be responsible for the highest CO conversion observed on ceria-supported catalysts.[23] Furthermore, theoretical studies have shown that only cationic gold (Au^+) can bind CO strongly enough to achieve CO oxidation.[15,24]

The gas phase association reactions of Au^+ with CO to form $Au^+(CO)_n$ have also been investigated, and some of these species are found to be stable at room temperature.[25-27] For example, Ozin *et al.* studied the gas phase interactions of neutral gold atoms with a CO/O_2 mixture using a matrix isolation experiment.[28] They reported the formation of an $Au(CO)_2(O_2)$ stable carbonate complex and its conversion at very low temperatures (40 K) to CO_2 and OAu(CO).[28] Hagen *et al.* also reported the formation of anionic complexes, such as $Au_2^-(CO)O_2$, $Au_3^-(CO)O_2$, and $Au_3^-(CO)(O_2)_2$, as intermediates in the catalytic CO oxidation over negatively charged Au clusters.[29]

To understand the reaction mechanism of CO oxidation on Au based catalysts it is important to study the gas phase reactions of Au^+ with CO, O_2, and their mixture given that moisture and impurities such as hydrocarbons present on the surface of a nanoparticle catalyst are known to modify its catalytic activity. On the other hand, water has been found to promote and enhance the low-temperature CO oxidation of atomic-oxygen covered Au(111)[30] and Pt(111) surfaces.[31] Water was found to either stabilize the transition state through hydrogen bonding, thus reducing the energy barrier or to dissociate into H and OH and then actively participate by inducing new more favorable reaction mechanisms.

In this paper, Laser Vaporization Ionization-High Pressure Mass Spectrometry (LVI-HPMS) and first principles *ab-initio* calculations are used to study the interaction between a singly charged Au^+ ion and small molecules such as CO, O_2, CO/O_2 mixture and H_2O. Unlike high vacuum mass spectrometric experiments, the LVI-HPMS technique allows for collisional stabilization of the activated complexes and therefore, intermediate and final products of the sequential and consecutive reactions of these molecules with the gold cation can be observed.[32-34] At a pressure of one Torr at 300 K, the number of collisions the gold cation experiences with the carrier gas atoms and the reactant neutral molecules during a reaction time of 5 millisecond is about 10^4 collisions which is more than sufficient to ensure thermalization of the gold cations and stabilization of the activated complexes.[32-34] Using the LVI-HPMS, we are especially interested in studying the function of Au^+ as a potential low temperature catalyst for CO oxidation in the presence of O_2 and how water may reduce or even poison the catalytic activity.

The atomic level understanding of these interactions will serve as a base for the design of novel nanocatalysts that are efficient under ambient conditions.

2. METHODS

2.1 Experimental

The gas phase reactions of a gold cation with several molecules were studied using the LVI-HPMS technique as described previously.[32-34] Gold cations were generated by focusing the output of the second harmonic of a Nd:YAG laser (532 nm, 22 mW of power pulsed at 10 Hz, laser spot 0.5 - 1 mm diameter and laser irradiance of ~ 7×10^7 W/ cm^2) on a gold rod placed in a high-pressure cell. The cell was a 2.5 cm × 2.5 cm aluminum cube mounted inside a high vacuum chamber as shown in Figure 1. The HPMS cell has two S1-UV windows where the laser beam enters and exits. The gas is introduced to the cell via a needle valve, and flows behind the entrance window of the cell to prevent any metal particle deposition over the window during the laser vaporization of the metal. When the laser beam strikes the gold rod, it vaporizes the metal and forms a plasma consisting of neutral metal atoms, metal ions, and electrons. The metal ions react with the neutral molecules forming excited or activated complexes which can be stabilized by collisions with the carrier gas (He). The products can be non-covalent association products or new covalent products resulting from chemical reactions of the activated complexes with neutral molecules.[32-34] The reaction products exiting the cell through a pinhole are focused by electrostatic lenses, analyzed by a quadrupole mass filter (Extrel C-50), and detected by an electron multiplier. The quadrupole mass spectrometer is controlled using an Extrel C-50 Controller with a mass range of 10-550 amu. The resolution of the quadrupole is better than 1 amu. The ion current from the electron multiplier is amplified and recorded. To collect the mass spectrum, the ion arrival time signal is gated using a boxcar integrator, averaged 5 times, and then recorded. To collect the arrival time of different species, the signal is recorded and averaged 200 times using a LeCroy 9450 oscilloscope.

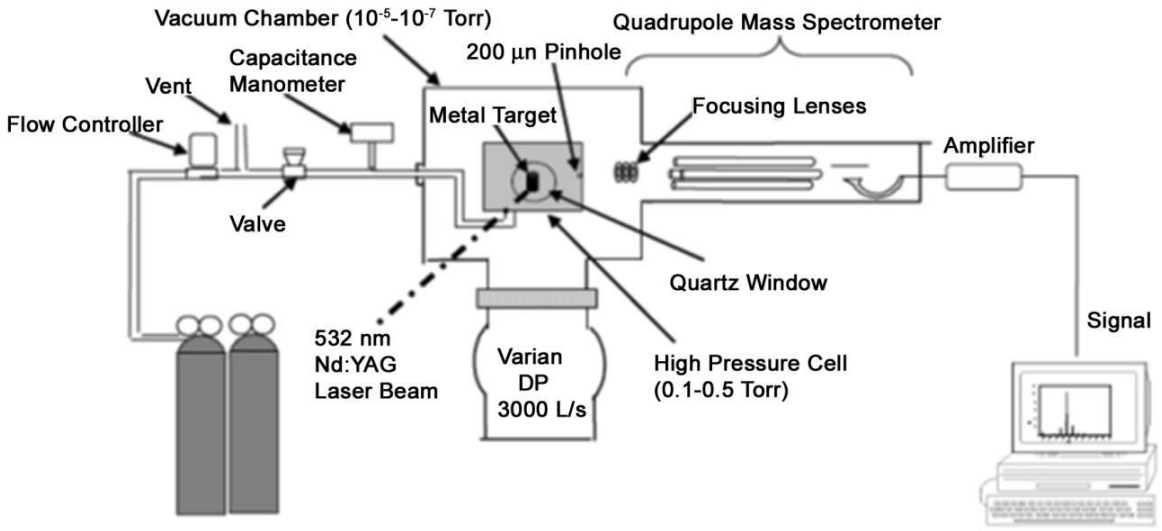

Figure 1. Schematic diagram of the Laser Vaporization Ionization High Pressure Mass Spectrometry (LVI-HPMS) system and relevant components.

2.2 Theoretical and Computational Methods

The theoretical calculations were carried out within a density functional theory (DFT) formalism and the generalized gradient approximation proposed by the revised PBE functional[35] proposed by Hammer *et al*. (PBE99).[36] The electronic orbitals and eigenstates were determined by using a linear combination of Gaussian atomic type orbital molecular orbital (LCGTO) approach in the deMon2k software.[37-38] For the H, C, N and O atoms we employed the DFT optimized DZVP basis set,[39] whereas the Au atom was described by a scalar relativistic effective core potential (ECP) with 19 valence electrons as proposed by Schwerdtfeger *et al.*,[40] in combination with the correlation consistent aug-cc-pVTZ-PP valence basis set.[41] The auxiliary density was expanded in primitive Hermite Gaussian functions using the GEN-A2 auxiliary function set for H, C, N and O atoms and the GEN-A2* auxiliary function set for Au.[42] The exchange-correlation potential was calculated with the orbital density. Given that the potential energy surface of the studied clusters is very flat, we employed a relative large adaptive grid[43] with a grid tolerance of 10^{-6} a.u., and a very tight convergence criteria for the converged self-consistent field (SCF) energy, root mean square (RMS) error = 10^{-6} a.u., and for the geometry optimization RMS force = $1.x10^{-4}$ a.u. To determine the ground state geometries the configuration space was sampled by starting from several initial configurations and fully

optimizing the geometries without symmetry constraints using a quasi-Newton method in redundant coordinates.[44] The resulting ground states were characterized via a frequency analysis and atomic charges were determined by a natural bond orbital (NBO) analysis.[45] Reported binding energies include the zero point energy correction. This methodology has been tested via studies on small water clusters $(H_2O)_n$ with n=2-5 and gold-water clusters $Au(H_2O)^+_n$ with n = 1-10 in which we found that our optimized structures[46] agreed well with the ones from existing high level *ab-initio* calculations,[47,48] and that the calculated binding energies, with an accuracy of around 1 kcal/mol, agreed well with the available experimental data.[49,50]

3. RESULTS AND DISCUSSION

To understand the reaction mechanism of CO oxidation on gold we investigated the gas phase reaction of Au^+ with CO, O_2, and a (3.4 % CO, 20 % O_2/ He) mixture as a function of pressure at room temperature using the LVI-HPMS technique. The gas phase reaction of Au^+ with the studied molecules resulted in successive addition reactions to the Au^+ core. Collisional stabilization was found to be a very important process in the metal ion-molecule reactions because when the ion and molecules collide in the gas phase and attempt to combine chemically, the product is formed in an excited state with an excess of vibrational energy. The newly formed product must then lose this energy to become stable or disassociate back to reactants if no stabilization occurs. Low pressure stabilization was generally accomplished by collisions with other species such as gases inside the cell, or via a radiative process.

3.1 Gas phase reaction of Au^+ with CO and CO oxidation to CO_2

CO reaction with the Au^+ ion resulted in successive addition with the formation of the $Au^+(CO)$, $Au^+(CO)_2$, and $Au^+(CO)(O_2)$ (due to O_2 impurity present with CO) complexes at low pressure. At high pressure, there was an addition of H_2O (also as a result of H_2O impurity) to $Au^+(CO)(O_2)$ and $Au^+(CO)_2$ as shown in Fig. 2. The proposed reaction scheme for Au^+ with CO is summarized as follows. At low pressures of pure CO, the reaction of the Au^+ with CO is dominated by an adduct formation where Au^+ reacts with CO to form the $[Au(CO)^+]^*$ excited complex which is stabilized by collision with other CO molecules to form $Au^+(CO)$ as shown in equation 1, where -ΔE is the calculated binding energy of $Au^+(CO)$.

$$Au^+ + CO \rightleftharpoons [Au^+(CO)]^* \longrightarrow Au^+(CO) \qquad \Delta E = -54.1 \text{ kcal/mol} \qquad (1)$$

This exothermic reaction is highly favored thermodynamically with a calculated binding energy (ΔE) of 54.1 kcal/mol. If no stabilization occurs $Au^+(CO)$ either vanishes or can be stabilized by further addition of another CO molecule to form $Au^+(CO)_2$ with a calculated large energy gain of 47.9 kcal/mol as shown in equation 2.

$$Au^+(CO) + CO \rightleftharpoons Au^+(CO)_2 \qquad \Delta E = -47.9 \text{ kcal/mol} \qquad (2)$$

Addition of a third CO molecule to Au^+ is much less favored with a calculated energy gain of only 4.8 kcal/mol. Moreover, $Au^+(CO)_3$ is not observed experimentally, which leads us to conclude that saturation of the gold cation (Au^+) is reached with two CO molecules. $[Au^+(CO)]^*$ can also be stabilized by either its reaction with impurities such as O_2 to form $Au^+(CO)(O_2)$ followed by the addition of H_2O to form $Au^+(CO)(H_2O)(O_2)$, as shown in equations 3 and 4 with calculated binding energies of 17.7 kcal/mol and 31.1 kcal/mol, respectively. At high pressures (100 mTorr), $Au^+(CO)(O_2)$ also adds another O_2 molecule to form $Au^+(CO)(O_2)_2$ as shown in Figure 2 and illustrated by equation 5.

$$Au^+(CO) + O_2 \rightleftharpoons Au^+(CO)O_2 \qquad \Delta E = -17.7 \text{ kcal/mol} \qquad (3)$$

$$Au^+(CO)(O_2) + H_2O \rightleftharpoons Au^+(CO)(H_2O)(O_2) \qquad \Delta E = -31.1 \text{ kcal/mol} \qquad (4)$$

$$Au^+(CO)(O_2) + O_2 \rightleftharpoons Au^+(CO)(O_2)_2 \qquad \Delta E \sim -1.0 \text{ kcal/mol} \qquad (5)$$

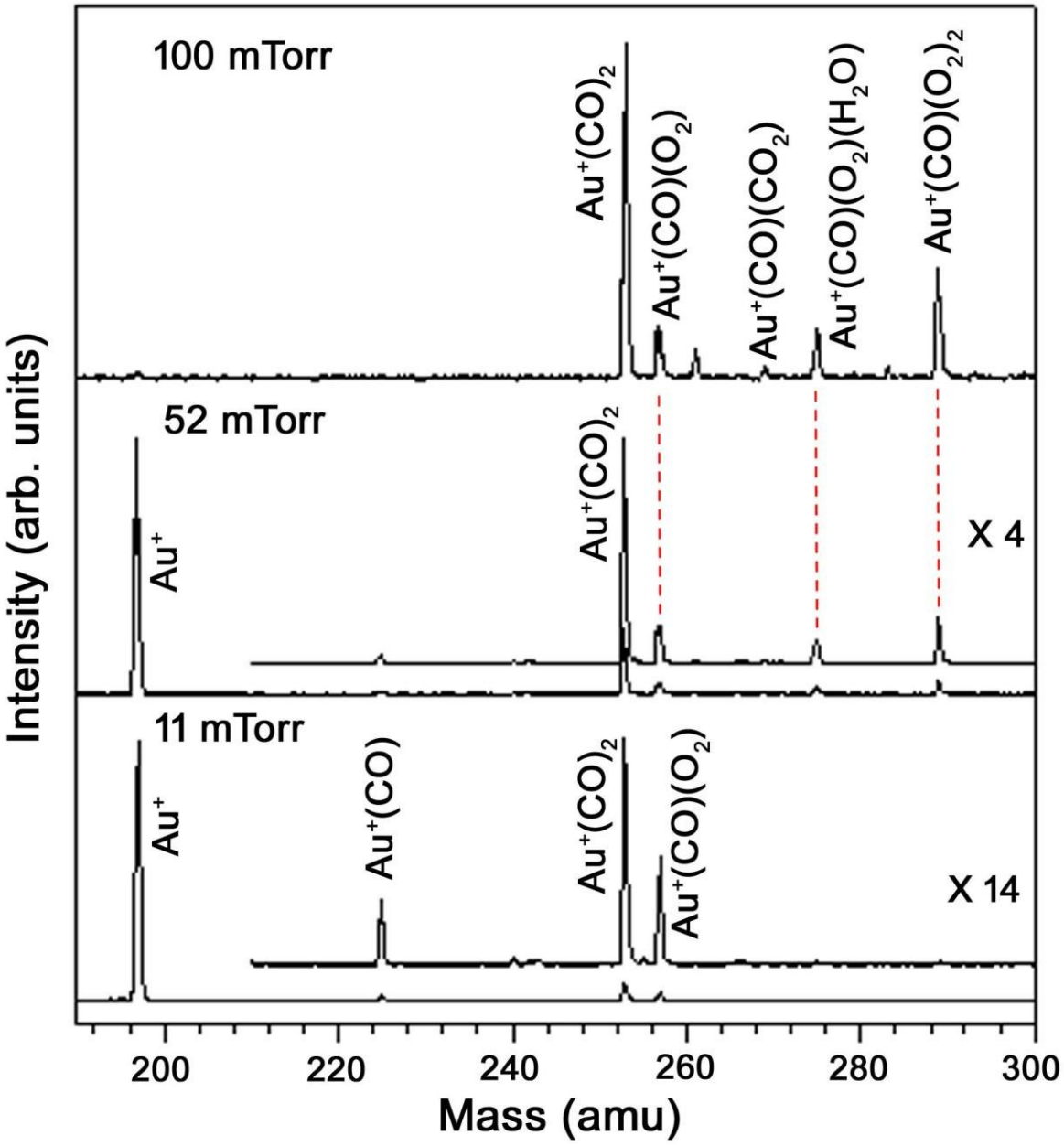

Figure 2. Mass spectra of the gas phase reactions of Au^+ with CO at different pressures as shown in the presence of trace impurities of O_2 and H_2O at 298 K.

All the major products observed in Fig. 1 can be explained by the calculated exothermic reactions 1-5. The optimized geometries of the products and energy changes for each reaction

step are shown in Fig. 3. According to our calculations, the order of Au^+ binding energy is as follows: $\Delta E(CO) > \Delta E(H_2O) > \Delta E(O_2)$. That is, CO binds the strongest to Au^+, followed by H_2O, and then by O_2 in agreement with the experimental results. We found that Au^+ coordination can be extended to have two CO and one O_2 molecule directly attached as seen in $Au^+(CO)_2(O_2)$ in Fig. 3.

The observation of $Au^+(CO)(O_2)$ in the mass spectra of Figure 2 formed by reaction (3) suggests that at high pressures $Au^+(CO)(O_2)$ could react with CO to form $Au^+(CO)_2(O_2)$ (not observed) which reacts with another CO molecule to form $Au^+(CO)(CO_2)$ + CO_2. This is consistent with the observation of $Au^+(CO)(CO_2)$ with a small intensity at 100 mTorr pressure as shown in Fig. 2. However, $Au^+(CO)(O_2)$ also reacts with H_2O in a highly exothermic reaction (-31 kcal/mol, equation 4) to form $Au^+(CO)(H_2O)(O_2)$ as shown in Fig. 2. This clearly shows that the presence of a trace amount of water prevents the formation of the $Au^+(CO)_2(O_2)$ reactive intermediate due to the formation of the competing product $Au^+(CO)(H_2O)(O_2)$ as observed in Fig. 2.

Experimental and theoretical data have shown that the Eley-Rideal mechanism is responsible for the CO oxidation on small gas phase clusters.[15,51-54] In this mechanism only one molecule (CO or O_2) absorbs and the other one reacts directly within the associated complex formed in the gas phase. In the case of O_2 absorption the reaction is determined by a partial electron transfer from the metal cluster to the anti-bonding π-orbital of the oxygen molecule which forms an activated superoxide species with stretched O-O bond length of more than 1.31 Å.[55] In our case CO and O_2 were found to be co-absorbed on Au^+ (reaction 3) but the presence of water leads to the highly exothermic reaction (4) which competes favorably with the addition of a second CO molecule to assist in the activation of O_2 within the $Au^+(CO)_2(O_2)$ complex which reacts further with CO to produce $Au^+(CO)(CO_2)$ + CO_2. This mechanism is consistent with the results of Ozin *et al.*[28] of CO oxidation on Au neutral atoms. According to Ozin *et al.* [28], the CO oxidation reaction proceeds after the addition of two molecules of CO to the Au atom and the reaction of $Au(CO)_2$ with one molecule of O_2 to form the neutral carbonate $Au(CO)_2(O_2)$ complex which assists the conversion of CO to CO_2 at low temperatures (30-40 K). According to our calculations reaction of $Au^+(CO)_2$ with O_2 leads to the formation of a weakly bound complex with an unaltered O_2 molecule bound at a large distance of 3.38 Å from the Au^+ core, as shown in Fig. 3, and with a very small energy gain as shown in equation 6:

$$Au^{+}(CO)_2 + O_2 \rightleftharpoons Au^{+}(CO)_2(O_2) \qquad \Delta E = -2.7 \text{ kcal/mol} \qquad (6)$$

Furthermore, the presence of a small trace of water added to $Au^{+}(CO)_2(O_2)$ and the consequent replacement of O_2 by H_2O prevent the formation of the $Au^{+}(CO)_2(O_2)$ intermediate in sufficient concentration.

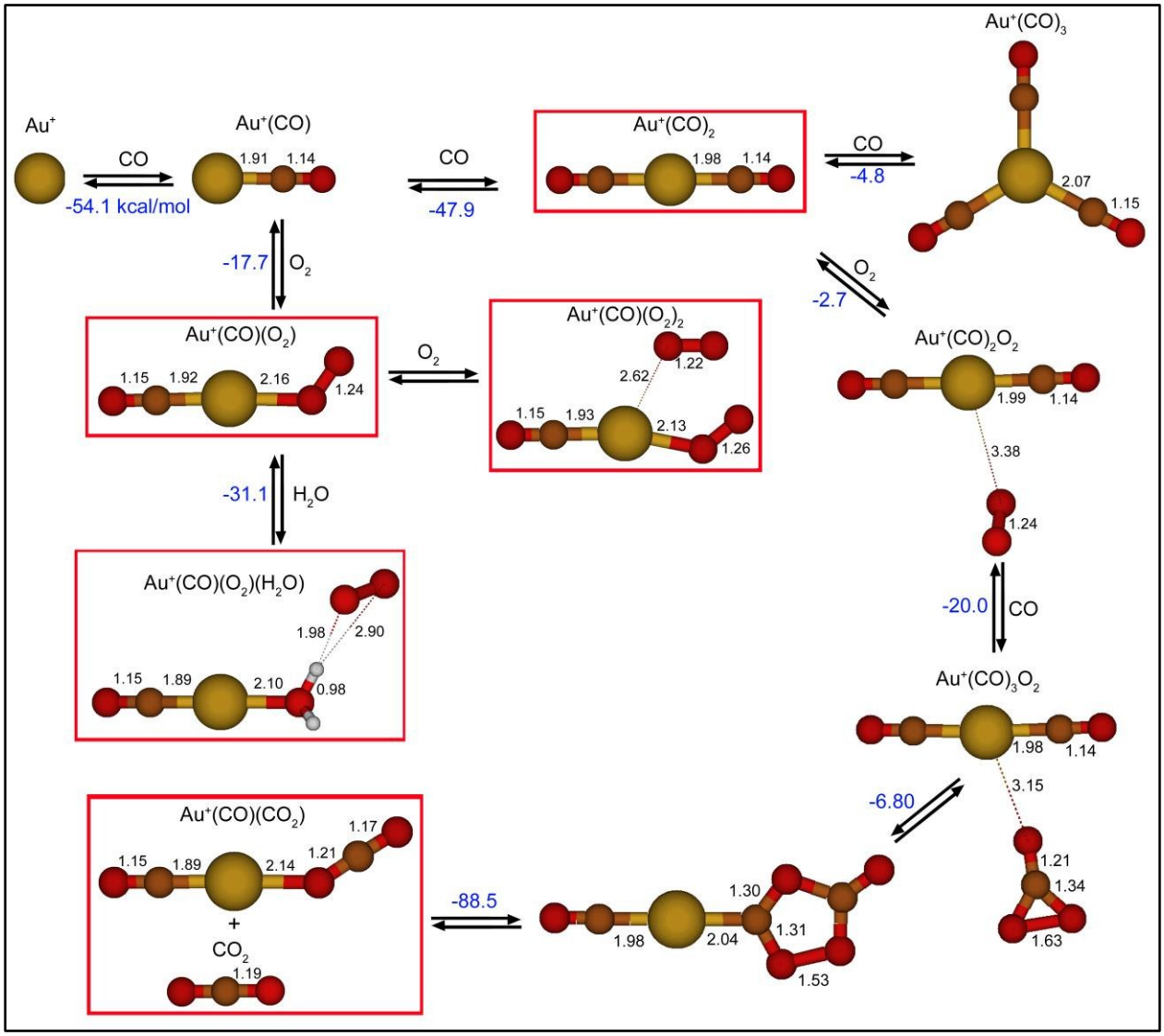

Figure 3. Summary of the reactions of Au^{+} with CO in the presence of O_2 and H_2O molecules, energy changes are given kcal/mol. Optimized geometries of all species are shown and the main products observed experimentally are marked with a red square. Yellow, red, brown and white circles represent gold, oxygen, carbon, and hydrogen atoms respectively. Bond lengths are given in Angstroms.

3.2 Gas phase reactions of Au^+ with O_2

The reaction of Au^+ with O_2 at low pressure (37 mTorr) resulted in the formation of the $Au^+(O_2)$ complex as shown in Fig. 4. However, due to the presence of H_2O and N_2 impurities other products such as $Au^+(H_2O)_{1-2}$, $Au^+(N_2)$ and $Au^+(N_2)(H_2O)$ are also observed. As the pressure increased to 100 mTorr, $Au^+(O_2)$ disappeared and only the clusters of H_2O on the Au^+ ion $Au^+(H_2O)_n$, with n =1-5 are observed as shown in Fig. 4.

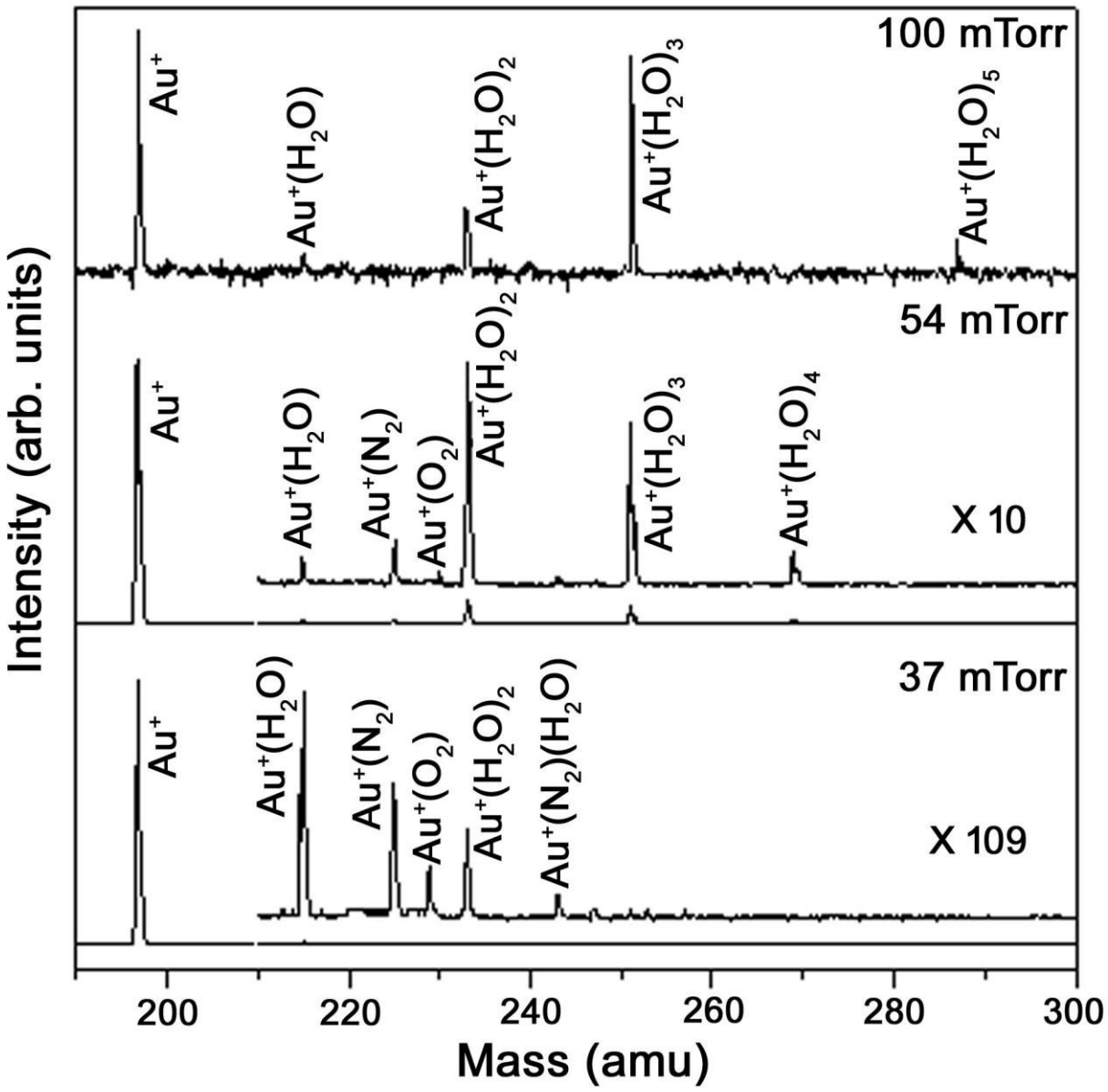

Figure 4. Mass spectra of the gas phase reactions of Au^+ with O_2 at different pressures as shown in the presence of trace impurities of N_2 and H_2O at 298 K.

The reaction scheme of Au^+ with O_2 can be summarized as follows. At low pressures of pure O_2, Au^+ reacts with O_2 to form the $[Au^+(O_2)]^*$ excited complex which is stabilized by collisions with O_2 molecules to form the $Au^+(O_2)$ complex with a calculated binding energy of 17.3 kcal/mol as shown in equation 7.

$$Au^+ + O_2 \rightleftharpoons [Au^+ + O_2]^* \longrightarrow Au^+(O_2) \qquad \Delta E = -17.3 \text{ kcal/mol} \qquad (7)$$

$Au^+(O_2)$ can then react with another O_2 to form the $Au^+(O_2)_2$ complex with a slightly higher binding energy than that of the $Au^+(O_2)$ complex as shown in equation 8.

$$Au^+(O_2) + O_2 \rightleftharpoons Au^+(O_2)_2 \qquad \Delta E = -17.8 \text{ kcal/mol} \qquad (8)$$

Additions of N_2 and H_2O were also observed due to the presence of impurities in the O_2 tank. N_2 binds more strongly than O_2 to Au^+ as shown in equation 9, and this is the reason that it presents a higher intensity signal in the mass spectra shown in Fig. 4.

$$Au^+ + N_2 \rightleftharpoons Au^+(N_2) \qquad \Delta E = -27.2 \text{ kcal/mol} \qquad (9)$$

H_2O impurities also react with Au^+ to form $Au^+(H_2O)$. At high O_2 pressure (100 mTorr), $Au^+(O_2)$ and $Au^+(N_2)$ vanished and the mass spectrum was dominated by the successive addition of H_2O on Au^+ to form $Au^+(H_2O)_n$ clusters with n = 1-5, as shown in Fig. 4.

The summary of the reactions of Au^+ with O_2 in the presence of trace impurities of N_2 and H_2O is shown in Fig. 5. As noted before the binding energy of H_2O to Au^+ is higher than the binding of O_2, and it is also higher than the binding of N_2. In particular, the first two H_2O molecules directly attach to Au^+ in the first coordination shell with a large energy gain of 39.6 and 42.6 kcal respectively. It is interesting that in case of O_2 and H_2O, Au^+ binds the second molecule more strongly than the first probably because the attachment of the first molecule alters the electronic states towards a more favorable interaction with the second molecule. This trend has been observed experimentally in the binding of other transition metal cations with water.[55] Additional H_2O molecules attach to the first solvation shell through hydrogen bonds resulting in sequential binding energies of 18.3, 16.4 and 13.5 kcal/mol for the third, fourth and fifth water molecules, respectively as shown in Fig. 5, in agreement with previous calculations.[46]

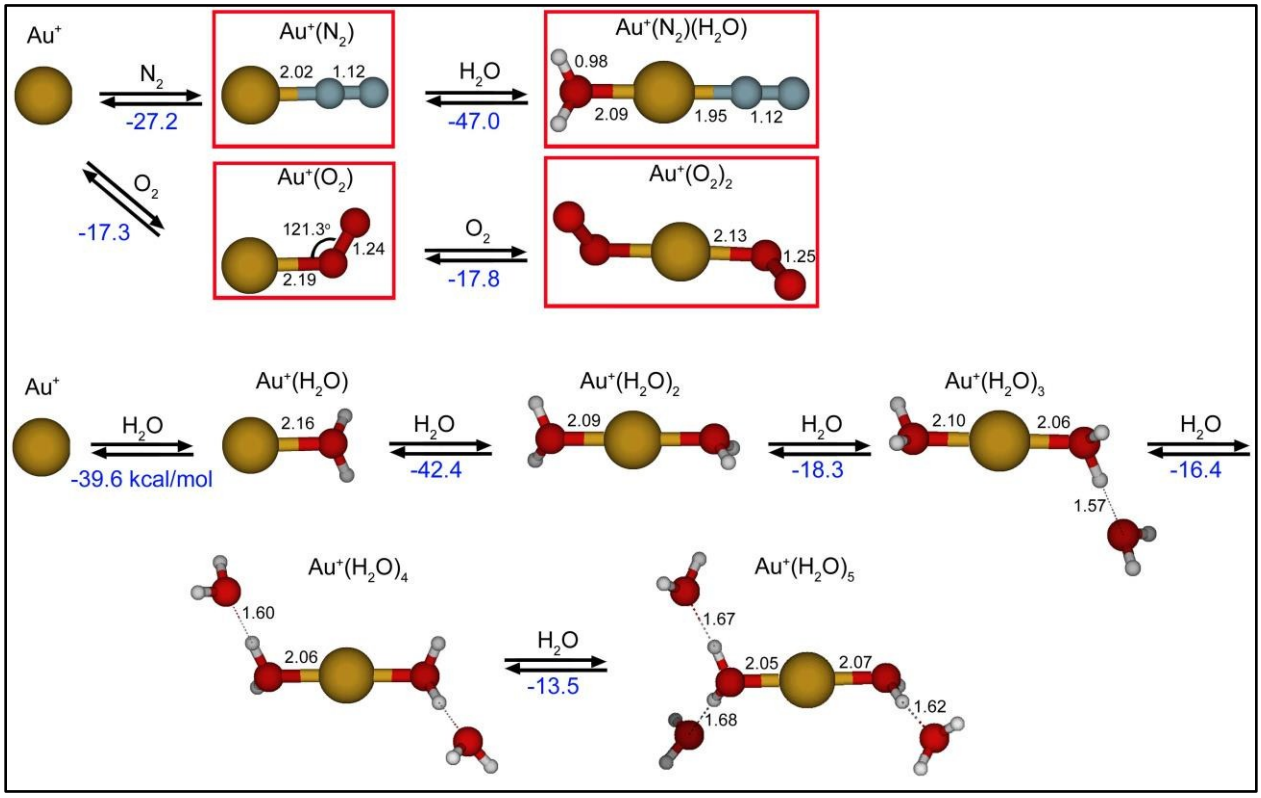

Figure 5. Summary of the reactions of Au^+ with O_2 and N_2 in the presence of H_2O, and the sequential clustering of five water molecules on Au^+, energy changes are given kcal/mol. Optimized geometries of all species are shown and the main products observed experimentally are marked with a red square.

3.3 Gas phase reactions of Au^+ with 3.4% CO, 20% O_2 / He mixture

The mass spectra resulting from the reactions of Au^+ with a 3.4% CO, 20% O_2/He mixture shows the formation of the $Au^+(CO)$, $Au^+(CO)_2$, $Au^+(CO)(H_2O)$, $Au^+(CO)(H_2O)_2$ and $Au^+(CO)(H_2O)_3$ species as shown in Fig. 6. However, the intermediate $Au^+(CO)_2(O_2)$ was not observed and only a small signal of $Au^+(CO)(CO_2)$ was detected as shown in Fig. 6. This again is consistent with the reaction of the intermediate $Au^+(CO)_2(O_2)$ with another CO to form $Au^+(CO)(CO_2)$ + CO_2 as explained in the analysis of the mass spectra shown in Fig. 2. Time profiles for the major observed species resulting from the reactions of Au^+ with CO/O_2 mixture in He containing a trace amount of water at 298 K are shown in Fig.7. It is clear from the observed time profiles that the Au^+ ion signal decays quickly following the reactions with CO and H_2O to form $Au^+(CO)_2$, $Au^+(CO)(H_2O)_2$, $Au^+(CO)(H_2O)_3$, and $Au^+(CO)(O_2)(H_2O)$. It is

important to also note the slow formation of $Au^+(CO)(CO_2)$ at a low concentration which seems to level off at the same time the formation of $Au^+(CO)(H_2O)(O_2)$ increases in intensity. This again, supports the assumption that the formation of $Au^+(CO)(H_2O)(O_2)$ by the addition of H_2O to $Au^+(CO)(O_2)$ prevents the formation of $Au^+(CO)_2(O_2)$ by the addition of CO to $Au^+(CO)(O_2)$. The formation and subsequent reaction of $Au^+(CO)_2(O_2)$ with CO appear to be the critical steps needed for the CO oxidation on gold ions to form $Au^+(CO)(CO_2) + CO_2$.

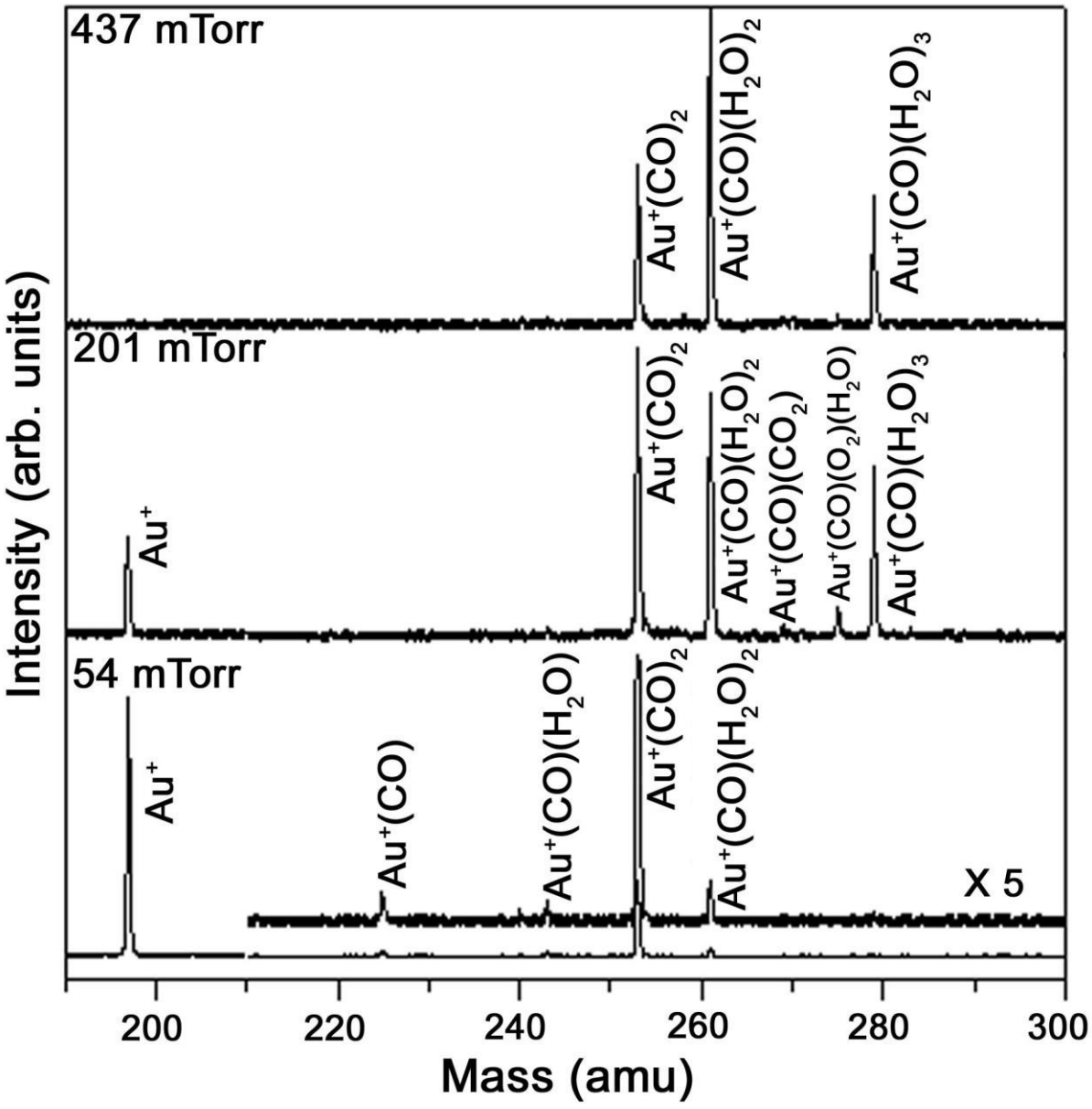

Figure 6. Mass spectra of the gas phase reactions of Au^+ with (3.4% CO, 20% O_2/He) mixture at different pressures as shown at 298 K.

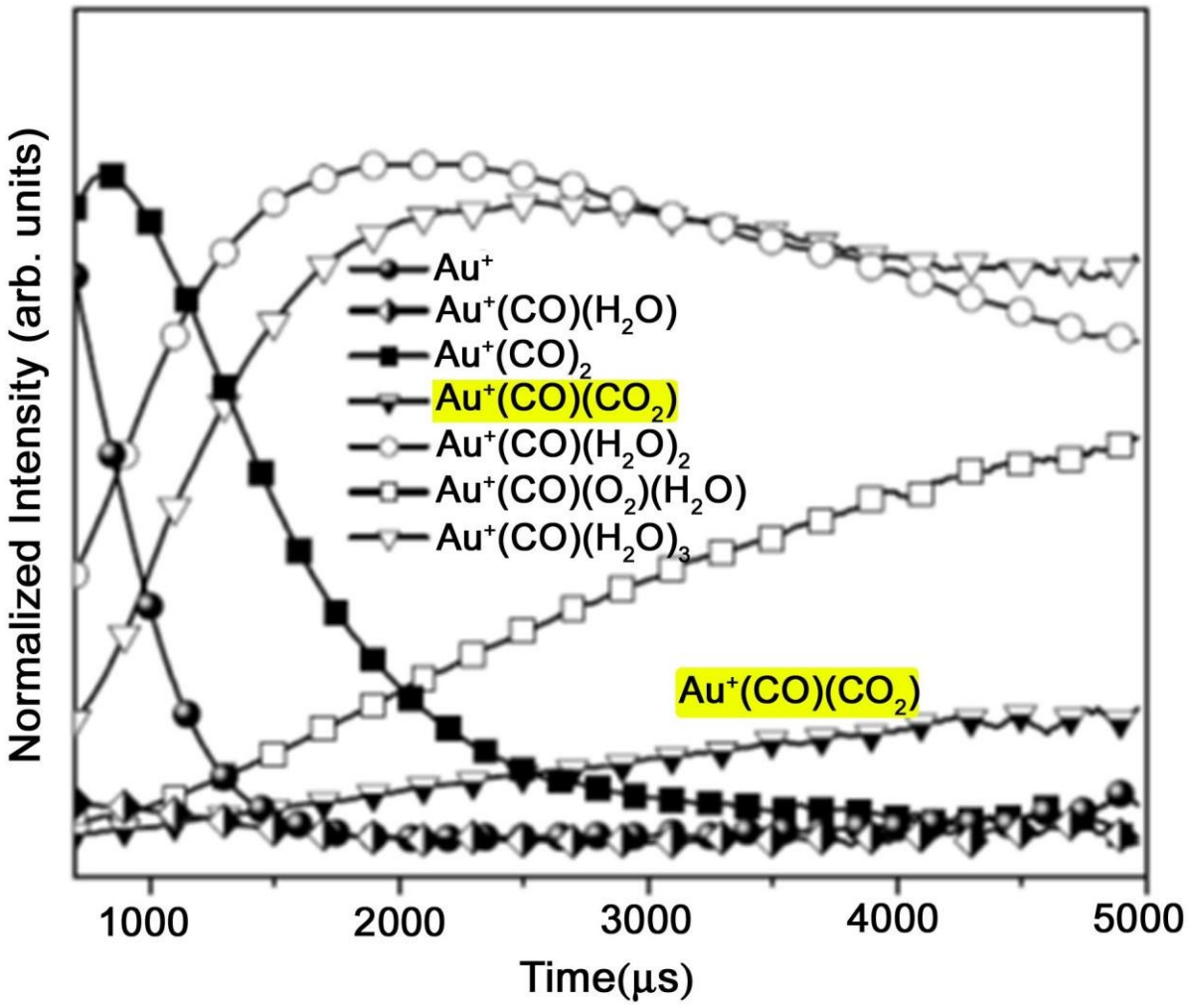

Figure 7. Normalized time profiles of major ions produced following the interaction of Au^+ ions with CO/O_2 mixture in He at 200 mTorr 298 K.

The summary of the reactions of Au^+ with the CO/O_2 mixture in the presence of trace water impurity and the structures of the stable products are given in Fig. 8.

The observations of $Au^+(CO)_2$, $Au^+(CO)(O_2)(H_2O)$ and $Au^+(CO)(CO_2)$ in the mass spectra of Fig. 6 and their reaction time profiles shown in Fig. 7 could provide evidence that the oxidation of CO on Au^+ occurs by the Langmuir-Hinshelwood (LH) mechanism.[15] The strong binding energies of the two CO molecules on Au^+ (54.1 and 47.9 kcal/mol) and the possible

addition of O_2 to form the reactive intermediate $Au^+(CO)_2(O_2)$ (not observed) could lead to a highly exothermic reaction (-115 kcal/mol) with another CO molecule to form $Au^+(CO)(CO_2)$ + CO_2 as shown in Fig. 8. The observation of the $Au^+(CO)(CO_2)$ complex supports the LH mechanism and is also consistent with previous gas phase experimental and theoretical studies which indicate that the oxidation of CO on cationic gold oxide clusters can occur by a Langmuir-Hinshelwood-like mechanism at multiple collision conditions as a result of the high adsorption energy of two CO molecules on AuO^+.[15]

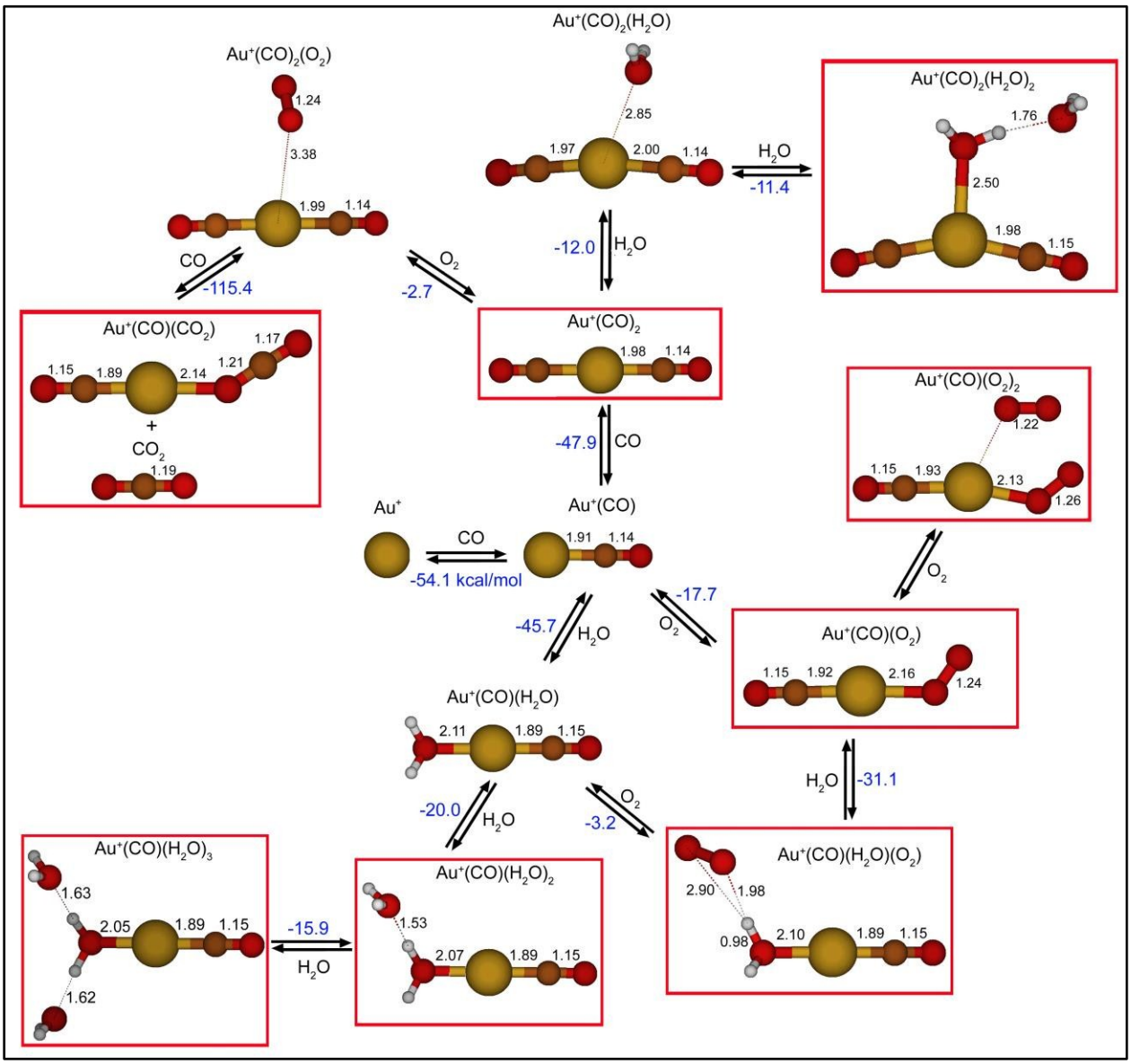

Figure 8. Summary of the reactions of Au^+ with (3.4% CO, 20% O_2/He) mixture, energy changes are given kcal/mol. Optimized geometries of all species are shown and the main products observed experimentally are marked with a red square.

3.4 Competitive binding of CO, H_2O, N_2, and O_2 to Au^+

As discussed above, the stoichiometry of the $Au^+(M)$ complex M = CO, H_2O, N_2, and O_2 is determined by the strength of the binding energy of Au^+ with the individual molecules. According to our calculations CO binds the strongest to Au^+, followed by H_2O, then N_2, and finally O_2, as given by equations 1, 10, 9 and 7:

$$Au^+ + CO \rightleftharpoons Au^+(CO) \qquad \Delta E = -54.1 \text{ kcal/mol} \qquad (1)$$

$$Au^+ + H_2O \rightleftharpoons Au^+(H_2O) \qquad \Delta E = -39.6 \text{ kcal/mol} \qquad (10)$$

$$Au^+ + N_2 \rightleftharpoons Au^+(N_2) \qquad \Delta E = -27.2 \text{ kcal/mol} \qquad (9)$$

$$Au^+ + O_2 \rightleftharpoons \longrightarrow Au^+(O_2) \qquad \Delta E = -17.3 \text{ kcal/mol} \qquad (7)$$

Figure 9 illustrates the competetion between the binding of CO, H_2O and O_2 to Au^+, and displays the structures of the product formed and the most liekly pathway for the CO oxidation on Au^+ in the presence of these molecules.

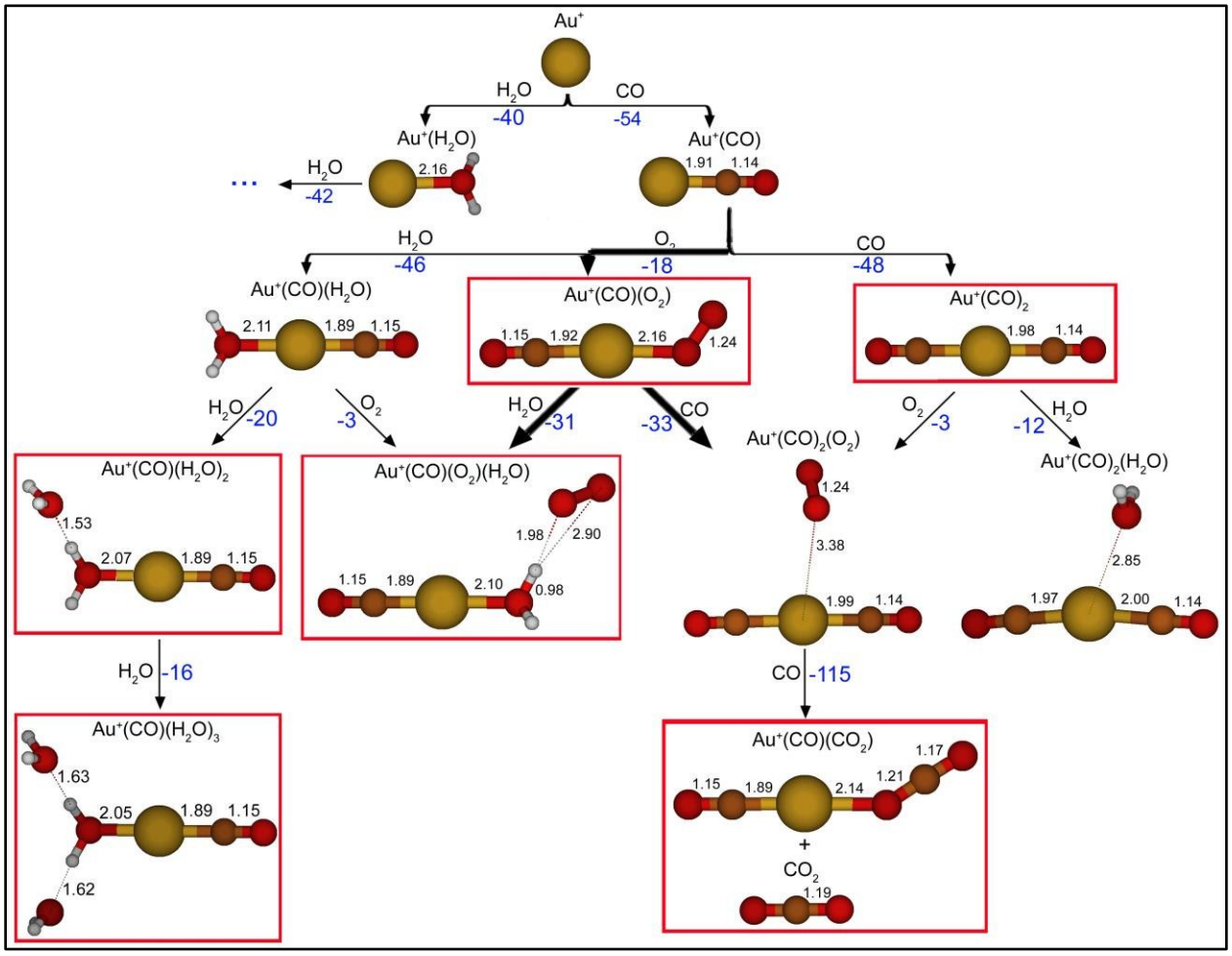

Figure 9. Summary of the reactions of Au^+ with CO, H_2O and O_2, energy changes are given kcal/mol. The main products observed experimentally are marked with a red square.

As discussed abvoe, the results suggest that the formation and subsequent reaction of $Au^+(CO)_2(O_2)$ with CO are the critical steps for the formation of $Au^+(CO)(CO_2)$ + CO_2. The most likely pathway proceeds by the association of O_2 into the $Au^+(CO)_2$ ion complex (-3 kcal/mol) to form $Au^+(CO)_2(O_2)$. We find that the subsequent addition of CO to $Au^+(CO)_2(O_2)$ results in a highly exothermic reaction (-115 kcal/mol) to form $Au^+(CO)(CO_2)$ + CO_2 as shown by equation 11.

$$Au^{+}(CO)_2(O_2) + CO \longrightarrow Au^{+}(CO)(CO_2) + CO_2 \quad \Delta E = -115 \text{ kcal/mol} \qquad (11)$$

This suggests that the intermedaite $Au^{+}(CO)_2(O_2)$ can act as an *auto-catalyst* for the oxidation of CO in the gas phase.

The binding energy order of CO, H_2O, N_2, and O_2 correlates with the chemical stability of the formed species as quantified by the calculated gap between the highest occupied and lowest unoccupied molecular orbitals (HOMO-LUMO gap): $Au^{+}(CO)_{\text{HOMO-LUMO gap}} > Au^{+}(H_2O)_{\text{HOMO-LUMO gap}} > Au^{+}(N_2)_{\text{HOMO-LUMO gap}} > Au^{+}(O_2)_{\text{HOMO-LUMO gap}}$. A large HOMO-LUMO gap is commonly used as an indicator of chemical stability, where the system resists both the change in the number of electrons and the deformation of the electronic cloud. Moisture and impurities present on the surface of a nanoparticle catalyst are known to modify the catalytic activity, and the atomic level understanding of the interaction between the active site, i.e. Au^{+} and the reactive species is therefore of paramount importance.

To investigate the origin of the difference in binding energies we analyzed the one-electron energy levels for Au^{+}, CO, $Au^{+}(CO)$, H_2O, $Au^{+}(H_2O)$, N_2, $Au^{+}(N_2)$, O_2 and $Au^{+}(O_2)$ as shown in Figure 10 and discussed below. The gold cation has an electronic configuration Au^{+}: **[**Xe**].**$4f^{\mathbf{14}}$**.**$5d^{\mathbf{10}}$ in which the relativistic effects led to stabilization of the 6s orbital and destabilization of the 5d orbitals, reducing the 5d-6s energy gap, to only 2.3 eV (see Fig. 10).[56] Hence, despite the fact that gold is known to be the noblest of all metals, nanoscale gold particles exhibits strong covalent bonding characters due to s-d hybridization and display a remarkable repertoire of chemistry.

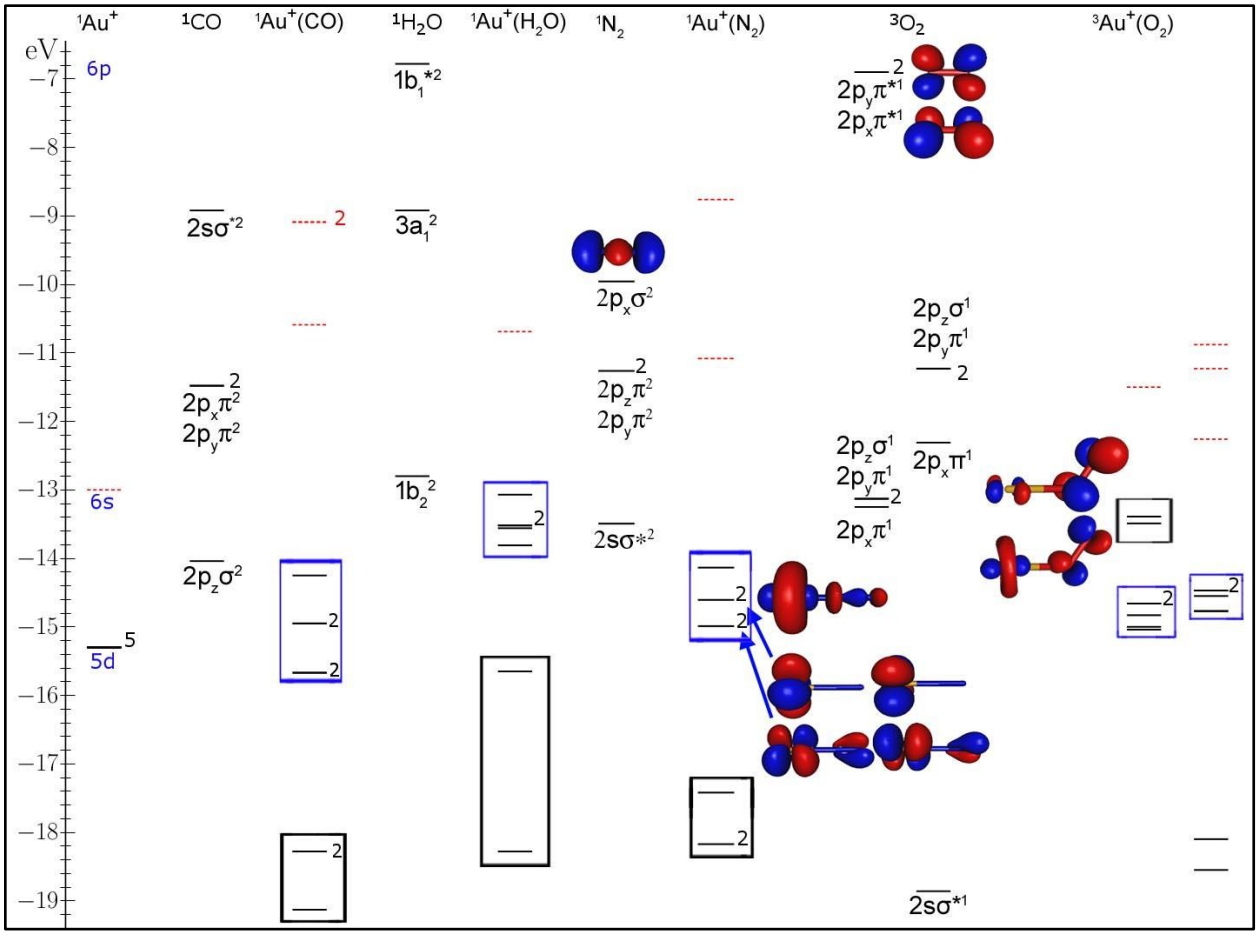

Figure 10. One electron energy levels of selected molecular orbitals of the Au^+, CO, $Au^+(CO)$, H_2O, $Au^+(H_2O)$, N_2, $Au^+(N_2)$, O_2, and $Au^+(O_2)$, species. For $Au^+(M)$, species M = CO, H_2O, N_2, and O_2. We have marked the energy levels with a significant contribution of the Au atom and of the M species with blue and black rectangles respectively. The continuous lines represent occupied levels, the dotted lines correspond to single unfilled states, the degeneracy is marked next to selected levels, and both the majority (up) and minority (down) spin states are shown. The highest occupied molecular orbitals are shown for O_2 and $Au(O_2)^+$ (isovalue = 0.1 au).

$Au^+(CO)$

CO molecule has an electronic configuration: $1s\sigma^2$ $1s\sigma^{*2}$ $2s\sigma^2$ $2p_z\sigma^2$ $2p_x\pi^2$ $2p_y\pi^2$ $2s\sigma^{*2}$ (Fig. 10). The binding mechanism of carbon monoxide on transition metals can be described within the Blyholder model,[57] which implies a double charge transfer between carbon monoxide and the metal: CO donates its lone-pair of σ electrons ($2s\sigma^{*2}$) into the 6s empty orbital of Au^+, while occupied 5d orbitals from Au^+ back-donate into the lowest unoccupied molecular orbital

(LUMO) of the CO molecule, which is an anti-bonding $2p\pi*$ orbital. The strength of these interactions (σ donation and π back-donation) depends on the orbital overlaps. Theoretical calculations suggest that CO binds stronger on gold cluster cations than on neutral and anionic clusters and that the forward donation (CO → metal) is the dominant mechanism in this case.[58] In our case $Au^+(CO)$ presented the largest binding energy (54.1 kcal/mol) and largest HOMO-LUMO gap (3.13 eV) compared to H_2O, N_2, and O_2. Further, Au^+ has the largest reduction of its atomic charge to only +0.76 while adopting a $6s^{0.57}$ $5d^{9.67}$configuration in the $Au^+(CO)$ complex as shown in Table 1.

$Au^+(H_2O)$

The $Au^+(H_2O)$ species presented a closed-shell configuration resulting from the interaction of Au^+ (^1S state) with the polar H_2O ($^1A_1$ state) molecule. Its bonding can be described as a combination of electrostatic ion/dipole interaction and significant covalent contributions. H_2O molecule has an electronic configuration: $1a_1^2$ $2a_1^2$ $1b_2^2$ $3a_1^2$ $1b_1^{*2}$ (Fig. 10) and bonding with Au^+ occurs by H_2O donation of its lone-pair $1b_1$ electrons ($1b_1^{*2}$) into the 6s empty orbital of Au^+, while occupied 5d orbitals from Au^+ back-donate into the anti-bonding $4a_1*$ lowest unoccupied molecular orbital (LUMO) of the H_2O molecule. Formation of $Au^+(H_2O)$ results in an energy gain of 39.6 kcal/mol forming a species with a large HOMO-LUMO gap of 2.38 eV. Attesting for the charge transfer from H_2O to Au^+ the atomic charge of Au reduces to +0.84 after Au adopts a $6s^{0.27}$ $5d^{9.89}$ configuration in $Au^+(H_2O)$ (Table 1).

$Au^+(N_2)$

N_2 is found to react with the Au^+ ion to form the closed-shell $Au^+(N_2)$ species through a combination of electrostatic ion/dipole and some covalent interactions. N_2 has an electronic configuration: $1s\sigma^2$ $1s\sigma^{*2}$ $2s\sigma^2$ $2s\sigma^{*2}$ $2p_y\pi^2$ $2p_z\pi^2$ $2p_x\sigma^2$ (Fig. 10). Bonding with Au^+ occurs by a partial donation of N_2 highest occupied molecular orbital ($2p_x\sigma^2$) to the 6s empty orbital of Au. Formation of $Au^+(N_2)$ results in an energy gain of 27.2 kcal/mol forming a species with a large HOMO-LUMO gap of 3.04 eV. Confirming the charge transfer from N_2 to Au^+ the atomic charge of Au reduces to +0.91 after which Au adopts a $6s^{0.29}$ $5d^{9.79}$ configuration and N_2 forms a dipole with -0.19 and 0.27 charges in each N atom in $Au^+(N_2)$ (Table 1). The top five highest occupied orbitals are of Au 5d character with some contributions from the N_2 orbitals, while the original N_2 are pushed down in energy in forming $Au^+(N_2)$ (Fig. 10).

$Au^+(O_2)$

The non-reactivity of cationic gold clusters (Au^+_n, $n \leq 20$) towards oxygen was previously observed by Cox *et al*. using a flow reactor technique.[60] Under the experimental conditions used for the measurements in this work we found the formation of $Au^+(O_2)$ at very low pressures, 37- 54 mTorr as shown in Fig. 4. In order to understand the low-reactivity of Au^+ towards molecular oxygen an analysis of the bonding mechanism is necessary. O_2 molecule electronic configuration is: $1s\sigma^2\ 1s\sigma^{*2}\ 2s\sigma^2\ 2s\sigma^{*2}\ 2p_x\pi^2\ 2p_y\pi^2\ 2p_z\sigma^2\ 2p_x\pi^{*1}\ 2p_y\pi^{*1}$ in which the degenerate antibonding $2p\pi*$ orbitals are half-filled. Oxygen being an oxidizing agent, usually acts as an electron acceptor, and the O_2 bonding to clusters occurs when an electron from the HOMO of the cluster is transferred into one of the anti-bonding $\pi*$ orbitals of O_2 molecule.[61] In the case of Au^+, which already has an electron less than neutral Au this charge transfer is energetically unfavorable. However, a covalent bonding interaction is found to occur between the 6s and 5d levels of Au and the $2p_x\pi$ orbitals of O_2, leading to the formation of $Au^+(O_2)$ with an energy gain of 17.3 kcal/mol in a species with a HOMO-LUMO gap of 1.13 eV. Further, this bonding results in the reduction of the atomic charge of Au to +0.9 after adopting a $6s^{0.25}\ 5d^{9.84}$ configuration in $Au^+(O_2)$ as summarized in Table 1. We should note that $Au^+(O_2)$ is an open shell system with a degenerate HOMO with main contributions of the $2p\pi^*$ oxygen anti-bonding orbitals. This explains the observed low stability of $Au^+(O_2)$, its disappearance as pressure increases, and the occurrence of the H_2O substitution reaction leading to the formation of a more stable the closed shell $Au^+(H_2O)$ species according to equation 12.

$$Au^+(O_2) + H_2O \longrightarrow Au^+(H_2O) + O_2 \qquad \Delta E = -22.4 \text{ kcal/mol} \qquad (12)$$

Table 1. Binding energies (ΔE) for the $Au^+ + M \rightarrow Au^+M$, (M = CO, H_2O, O_2, and N_2) reactions, electronic charges, electronic configuration, and HOMO-LUMO gap of the Au^+M species.

	ΔE (kcal/mol)	Electronic charge	Electronic Configuration	HOMO-LUMO gap (eV)
$Au^+(CO)$	54.1	**Au: 0.76**	Au [core] $6s^{0.57}$ $5d^{9.67}$	3.66
		C: 0.49	C [core] $2s^{1.27}$ $2p^{2.18}$	
		O: -0.26	O [core] $2s^{1.73}$ $2p^{4.49}$	
$Au^+(H_2O)$	39.6	**Au: 0.84**	Au [core] $6s^{0.27}$ $5d^{9.89}$	2.38
		O: -0.97	O [core] $2s^{1.77}$ $2p^{5.18}$	
		H: 0.56	H $1s^{0.43}$	
		H: 0.56	H $1s^{0.43}$	
$Au^+(N_2)$	27.2	**Au: 0.91**	Au [core] $6s^{0.29}$ $5d^{9.79}$	3.04
		N: -0.19	N [core] $2s^{1.51}$ $2p^{3.62}$	
		N: 0.27	N [core] $2s^{1.65}$ $2p^{3.04}$	
$Au^+(O_2)$	17.3	**Au: 0.90**	Au [core] $6s^{0.25}$ $5d^{9.84}$	1.13
		O: -0.10	O [core] $2s^{1.81}$ $2p^{4.25}$	
		O: 0.20	O [core] $2s^{1.83}$ $2p^{3.93}$	

4. CONCLUSIONS

We reported a detailed experimental and theoretical investigation of the gas phase reactivity of Au^+ with CO, H_2O, O_2, N_2 and their mixtures and the catalytic role of Au^+ towards CO oxidation. The gold cation is found to strongly interact with all present molecules and having successive addition reactions until reaching saturation. Au^+ reacts with CO to form stable $Au^+(CO)$ and $Au^+(CO)_2$ complexes. Trace impurities of H_2O were found to be added to Au^+ at high pressures in reactions that compete with the CO addition. The presence of water inhibits the formation of the carbonate $Au^+(CO)_2(O_2)$ intermediate thus preventing subsequent reaction with CO to form $Au^+(CO)(CO_2) + CO_2$. We found that the strength of the Au^+ binding energy with the neutral molecules is the key factor that determines the stoichiometry of the formed complexes and thus the possible poisoning of the catalyst. CO binds the strongest to Au^+, followed by H_2O, N_2 and then O_2. The current experiments and calculations might lead to a

molecular level understanding of the interactions between the active sites, reactants and impurities which could pave the way for the design of efficient nanocatalysts.

AUTHOR INFORMATION

Corresponding Author: mselshal@vcu.edu, Tel: +8048282753

Notes

The authors declare no competing financial interests.

ACKNOWLEDGEMENTS

We thank the National Science Foundation (CHE-1463989) for the support of this work. This research was partially supported by Virginia Commonwealth University (J.U.R.).

REFERENCES

1. Peden, C. H. F., Goodman, D. W., *J. Phys. Chem.* **1986**, *90*, 4839-4843.
2. Peden, C. H. F., Goodman, D. W., Weisel, M. D., Hoffmann, F. M. *Surf. Sci.* **1991**, *253*, 44-58.
3. Engel, T., Ertl, G. *Adv. Catal.* **1979**, *28*, 1-78.
4. Landman, U.; Yoon, B.; Zhang, C.; Heiz, U.; Arenz, M. *Top. Catal*. **2007**, 44, 145-158.
5. Harding, C.; Habibpour, V.; Kunz, S.; Farnbacher, A. N. S.; Heiz, U.; Yoon, B.; Landman, U. *J. Am. Chem. Soc*. **2009**, 131, 538-548.
6. Kane, M. D.; Roberts, F. S.; Anderson, S. L. *Inter. J. Mass Spetrom*. **2015**, 377, 263-277
7. Holland, P. M., Castleman, A. W., Jr. *J. Chem. phys.* **1982**, *76*, 4195.
8. Marinelli, P. J., Squires, R. R. *J. Am. Chem. Soc.* **1989**, *111*, 4101.
9. Daly, G. M..; El-Shall, M. S. *J. Phys. Chem.* **1995**, *99*, 5283.
10. Guo, B. C.; Castleman, A. W., Jr. *J. Am. Chem. Soc*. **1992**, 114, 6152.
11. Meot-Ner (Mautner), M.; Sieck, L. W.; El-Shall, M. S.; Daly, G. M. *J. Am. Chem. Soc*. **1995**, 117, 7737.
12. El-Shall, M. S. *Acct. Chem. Res.* **2008**, 41, 783-792.
13. Sharma, P.; Attah, I.; Momoh, P. O.; El-Shall, M. S. *Inter. J. Mass Spectrom.* **2011**, 300, 81-90.
14. Aysina, J.; Maranzana, A.; Tonachini, G.; Tosi, P.; Ascenzi, D. *J. Chem. Phys*. **2013**, 138, 204310.

15. Burgel, C.; Reilly, N. M.; Grant, E. Johnson, Mitric, R.; Kimble, M. L.; Castleman, A. W., Jr.; Bonacic-Koutecky, V. *J. Am. Chem. Soc*. **2008**, *130*, 1694-1698.
16. Somorjai, G. A. *Chem. Soc. Rev* **1984**, *13*, 321.
17. Ryabov, A. D. *Chem..Rev.* **1990**, *90*, 403.
18. Haruta, M.; Yamada, N.; Kobayashi, T.; Ijima, S. *J. Catal.* **1989**, *115*, 301.
19. Haruta, M.; Tsubota, S.; Kobayashi, T.; Kageyama, H.; Genet, M.; Delmon, B. *J. Catal*.**1993**, *144*, 175.
20. Minico, S.; Scire, S.; Crisafulli, C.; Visco, A.M.; Galvagno, S. *Catal. Lett.* **1997**, *47*, 273.
21. Park, E.D.; Lee, J.S. *J. Catal.* **1999**, *186*, 1.
22. Boyd, D.; Golunski, S.; Hearne, G.R.; Magadzu, T.; Mallick, K.; Raphulu, M.C.; Venugopal, A.; Scurrell, M.S. *Appl. Catal. A* **2005**, *292*, 76.
23. Venezia, A.M.; Pantaleo, G.; Longo, A.; Di Carlo, G.; Casaletto, M.P.; Liotta, F.L.; Deganello, G. *J. Phys. Chem. B* **2005**, *109*, 2821.
24. Liu, Z.P.; Stephen, J.J.; King, D.A. *Phys. Rev. Lett.* **2005**, *94*, 196102.
25. Willner, H., Aubke, F. *Inorganic Chemistry* **1990**, *29*, 2195.
26. Willner, H., Schaebs, J., Hwang, J., Mistry, F., Jones, R., Trotter, J., Aubke, F. *J. Am. Chem. Soc.* **1992**, *114*, 8972.
27. Lupinetti, A. J., Jonas, V., Thiel, W., Strauss, S. H., Frenking, G., *Chem. Europ. J.* **1999**, *5*, 2573.
28. McIntosh, D.; Ozin, G.A. *J. Org. Chem.* **1976**, *121*, 127.
29. Hagen, J., Socaciu, L. D., Elijazyfer, M., Hiez, U., Bernhardt, T. M., Woste, L. *Phys. Chem. Chem. Phys.* **2002**, *4*, 1707.
30. Ojifinni, R. A.; Froemming, N. S.; Gong, J.; Pan, M.; Kim, T. S.; White, J. M.; Henkelman, G.; Mullins, C. B. *J. Am. Chem. Soc.* **2008**, *130*, 6801-6812.
31. Gong, X. Q.; Hu, P.; Raval, R. *J. Chem. Phys.* **2003**, *119*, 6324-6334
32. Daly, G. M.; El-Shall, M. S. *J. Phys. Chem.* **1994**, *98*, 696-701.
33. Daly, G. M.; Pithawalla, Y. B.; Yu, Z.; El-Shall, M. S. *Chem. Phys. Lett.* **1995**, *237*, 97-105.
34. Pithawalla, Y. B.; McPherson, J.; El-Shall, M. S. *Chemical Physics Letters* **1999**, *309*, 215-220.
35. Perdew, J. P.; Burke, K.; Ernzerhof, M. *Phys. Re*V. *Lett*. **1996**, *77*, 3865.
36. Hammer, B.; Hansen, L. P.; Nørskov, J. K. *Phys. Re*V. *B.* **1999**, *59*, 7413.

37. Koster, A. M.; Calaminici, P.; Casida, M. E.; Flores-Moreno, R.; Geudtner, G.; Goursot, A.; Heine, T.; Ipatov, A.; Janetzko, F.; del Campo, J. M.; Patchkovskii, S.; Reveles, J. U.; Salahub, D. R.; Vela, A. deMon2k, Ver. 2.3.6; The deMon Developers, Cinvestav, Mexico (2010). Available at http://www.deMon-software.com
38. Geudtner, G.; Calaminici, P.; Carmona-Espindola, J.; M.del Campo, J.; Dominguez-Soria, V.D.; Flores Moreno, R.; Gamboa, G.U.; Goursot, A.; Koster, A.M.; Reveles, J.U.; Mineva, T.; Vazquez, J.M.; Vela, A.; Zuniga-Gutierrez, B.; Salahub, D.R. *WIREs Comp. Mol. Sci.* **2011**, DOI: 10.1002/wcms.98.
39. Godbout, N.; Salahub, D. R.; Andzelm, J.; Wimmer, E. *Can. J. Chem.* **1992**, *70*, 560.
40. Schwerdtfeger, P.; Dolg, M.; Schwarz, W. H. E.; Bowmaker, G. A.; Boyd, P. D. W. *J. Chem. Phys.* **1989**, *91*, 1762.
41. http://www.emsl.pnl.gov/forms/basisform.html.
42. Calaminici, P.; Janetzko, F.; Köster, A. M.; Mejia-Olvera, R.; Zúñiga-Gutierrez, B. *J. Chem. Phys.* **2007**, *126*, 044108.
43. Köster, A. M.; Flores-Moreno, R.; Reveles, J. U. *J. Chem. Phys.* **2004**, *121*, 681.
44. Reveles, J. U.; Köster, A. M. J. Comput. Chem. 2004, 25, 1109.
45. Reed, A. E.; Weinstock, R. B.; Weinhold, F. *J. Chem. Phys.* **1985**, *83*, 735.
46. Reveles, J. U.; Calaminici, P.; Betran, M. R.; Köster, A. M.; Khanna, S. N. *J. Am. Chem. Soc.* **2007**, *129*, 15565-15571.
47. Day, M. B.; Kirschner, K. N.; Shields, G. C. *J. Phys. Chem. A* **2005**, *109*, 6773.
48. Feller, D.; Glendening, E. D.; de Jong, W. A. *J. Chem. Phys.* **1999**, *100*, 1475.
49. Curtiss, L. A.; Frurip, D. J.; Blander, M. *J. Chem. Phys.* **1979**, *71*, 2703.
50. Poisson, L.; Lepetit, F.; Mestdagh, J. -M.; Visticot, J.-P. *J. Phys. Chem. A* **2002**, *106*, 5455.
51. Socaciu, L.D.; Hagen, J.; Bernhardt, T.M.; Wöste, L.; Heiz, U.; Häkkinen, U.; Landman, U. *J. Am. Chem. Soc.* **2003**, *125*, 10437.
52. Reilly, N.M.; Reveles, J.U.; Johnson, G.E.; Khanna, S.N.; Castleman Jr., A.W. *Chem. Phys. Lett.* **2007**, *435*, 295.
53. Reveles, J.U.; Johnson, G.E.; Khanna, S.N.; Castleman Jr., A.W. *J. Phys. Chem. C* **2010**, *114*, 5438.
54. Zamora, A.Y.; Reveles, J.U.; Mejia-Olvera, R.; Baruah, T.; Zope, R.R. Chem. Phys. Lett. **2014**, *612*, 117–123.

55. Dalleska, N. F.; Honma, K.; Sunderlin, L. S.; Armentrout, P. B. *J. Am. Chem. Soc.***1994**, *116*, 3519-3528.
56. Wang, L.-S. *Phys. Chem. Chem. Phys.* **2010**, *12*, 8694–8705
57. Häkkinen, U.; Landman, U. *J. Am. Chem. Soc.* **2001**, *123*, 9704.
58. Blyholder, G. *J. Phys. Chem.* **1964**, *68*, 2772-2778.
59. Wu, X.; Senapati, L.; Nayak, S. K.; Selloni, A.; Hajaligol, M. *J. Chem. Phys.* **2002**, *117*, 4010-4015.
60. Cox, D. M.; Brickman, R.; Creegan, K.; Kaldor, A. *Z. Phys. D - Atoms,Molecules and Clusters* **1991,** *19*, 353-355.
61. Lee, T. H.; Ervin, K. M. *J. Phys. Chem.* **1994,** *98*, 10023-10031.

Graphical Abstract